Experimental, numerical and theoretical investigations of Tesla turbines

Stefan Klingl[a,1], *Stefan* Lecheler[a] , and *Michael* Pfitzner[b]

[a] Department of Technical Thermodynamics, Faculty of Mechanical Engineering, Bundeswehr University Munich, Germany
[b] Institute of Thermodynamics, Faculty of Aviation and Aerospace Engineering, Bundeswehr University Munich, Germany

Abstract. We use analytical, numerical and experimental methods to characterize the laminar flow inside a Tesla turbine rotor gap. A comparison based on one particular set of operating conditions mutually validates the three approaches. The simplicity of the analytical flow model allows for a cost efficient optimization of the underlying turbine parameters. Performance charts exhibit general trends and serve as a guide for preliminary turbine design and optimization. In terms of the ratio of half the gap width to inlet radius and the ratio of outlet- to inlet radius, the designer of a tesla turbine has to find a compromise between optimal efficiency and optimal power output.

1 Introduction

A Tesla turbine uses the friction of a working fluid on the surfaces of multiple closely spaced disks (see Fig. 1) to generate torque. With this simple and robust design, friction-type turbomachinery might be a considerable competitor to conventional turbomachinery in certain niche fields of application, e.g. harvesting of industrial waste energy. However, an industrially viable design approach for friction turbines still does not exist. The first important step towards this goal is to fully understand their flow physics. In this context, the present study summarizes the analytical, numerical and experimental research done at the authors' institutes and performs a brief parameter study based on the analytical approach.

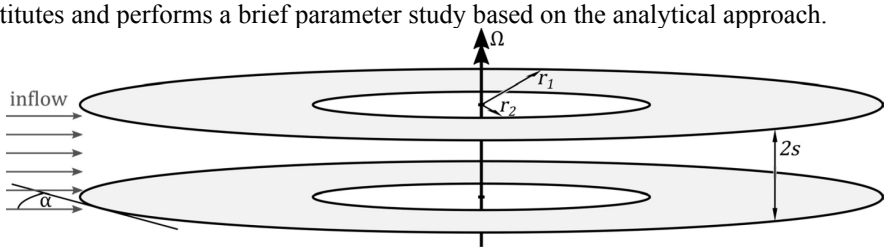

Fig. 1 Tesla turbine rotor with two disks

[1] Corresponding author: stefan.klingl@unibw.de

2 Flow modeling and validation

2.1 Analytical modeling

In order to model the flow inside the Tesla Turbine gap analytically, the governing conservation equations have to be simplified. Batista [1] assumes stationary, incompressible flow that is rotationally symmetric about the axis of rotation of the disks. He uses a velocity potential to absorb the continuity equation into the momentum equations and approximates the unknowns with truncated series expansions. A system of differential equations emerges that can be solved sequentially for the series coefficients. The present study further develops this approach.

For a start, the resulting expressions for pressure and velocities are large, unwieldy expressions that do not allow any conclusions on the dependences on the characteristic parameters upon visual inspection. Hence, a subsequent Taylor expansion clarifies the solutions and reveals for instance that the assumption of parabolic velocity profiles is strictly speaking only valid for the radial velocity component.

Another drawback of the original Batista [1] model is that it does not accommodate an arbitrary inlet boundary condition for the tangential velocity component. It is however possible to introduce a correction function into the truncated solution that creates an additional degree of freedom for said boundary condition. Schosser et al. [2] provides a detailed derivation and analysis of this idea.

Lastly, this study introduces an optimized non-dimensionalization, which aims for non-dimensional parameters that are as expressive as possible. The inlet radius r_1, half the gap width s, the radial inlet velocity u_{r1} and the fluid density ρ normalize velocities and pressure:

$$U = \frac{u_\phi}{u_{r1}}, \quad V = \frac{u_r}{u_{r1}}, \quad W = \frac{u_z}{u_{r1}}, \quad P = \frac{p}{\rho u_{r1}^2} \tag{1}$$

The indices ϕ, r and z indicate the tangential, radial and axial direction respectively. Lowercase letters (u and p) denote velocity and pressure while uppercase letters stand for their dimensionless counterparts. The independent variables in the mathematical model are the radial and axial spatial coordinate (r and z). Again, uppercase letters represent their normalized form.

$$R = \frac{r}{r_1}, \quad Z = \frac{z}{s} \tag{2}$$

Upon insertion into the system of equations, the following non-dimensional turbine parameters emerge:

$$\sigma = \frac{s}{r_1}, \quad Re = \frac{u_{r1} s}{\nu}, \quad U_1 = \frac{u_{\phi 1}}{u_{r1}}, \quad R_2 = \frac{r_2}{r_1}, \quad \Omega = \frac{r_1 \omega}{u_{r1}} \tag{3}$$

Where ν is the kinematic viscosity, ω the rotational speed and r_2 the outlet radius. The inlet angle α is related to U_1 in the following way.

$$\alpha = \arctan(\mathrm{U}_1^{-1}) \tag{4}$$

$\alpha = 0°$ corresponds to the tangential and $\alpha = 90°$ to the radial direction.

2.2 Numerical modeling

Numerical results using ANSYS CFX provide validation and additional information about the flow inside the rotor gap of a Tesla turbine. Similar to the analytical model, stationary, incompressible and rotationally symmetric laminar flow is specified. A 10°-sector of a flat annulus represents the fluid domain in the rotor gap and a structured grid with 30 elements along half the gap width is applied. The boundaries consist of inlet and outlet in the radial direction, rotational periodicity in the tangential direction as well as rotating wall and

symmetry in the axial direction. The velocity profile at the inlet assumes the shape of the analytical velocity profile.

2.3 Experimental validation

Particle tracking velocimetry (PTV) measurements are conducted on a test facility with a single, optically accessible friction turbine gap. In contrast to many of the earlier experimental studies, the ratio of gap width to diameter of the test rotor gap is realistically small. Schosser [3, 4] describes the test setup and -results in detail. The turbine stator mimics rotationally symmetric inflow with 36 equally distributed nozzles that provide compressed air to the rotor. Measurements in laminar as well as in transitional and turbulent regimes provide an extensive set of velocity profiles at two different radii inside the rotor gap.

2.4 Results and comparison

The comparison of the analytical, numerical and experimental results is based on a single, fully laminar operating point. Table 1 shows the important operating parameters.

Table 1 Selected operating conditions.

mass flow	$\dot{m}$	3.12	g/s
Reynolds number	Re	105	$-$
rotational speed	n	1000	$1/min$
	Ω	1.98	$-$
outlet radius	r_2	30	mm
	R_2	0.24	$-$

inlet radius	r_1	125	mm
gap width	$2s$	0.5	mm
	σ	0.002	$-$
inlet angle	α	21.3	°
density	ρ	1.15	kg/m^3
dynamic viscosity	μ	18.2	$\mu Pa\ s$

Fig. 2 and Fig. 3 show the radial and tangential velocity profiles from all three approaches respectively. The inlet angle $\alpha = 21.3°$ is chosen so that the theoretical curves match the experimental point cloud at the outermost examined radius $R = 0.8$ (see Fig. 2 left). The geometric inlet angle, defined by the tips of the stator blades is 12.1°.

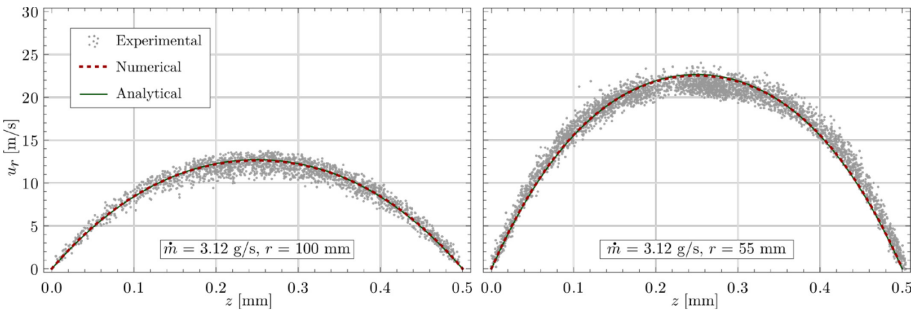

Fig. 2 Radial velocity profiles at $r = 100mm$ ($R = 0.80$) and $r = 55mm$ ($R = 0.44$).

Since the analytical and numerical solutions are barely distinguishable in all four charts, the analytical approach models the flow sufficiently well at the examined operating point. The scattering of the experimental data is not yet fully understood and only partially caused by measurement error. Possible explanations range from instationary flow structures to vibration and deformation of the rotor during operation. Apart from that, all velocity profiles agree well. At the inner radius, the theoretical tangential velocity deviates slightly from the experimental one (see Fig. 3 right). This confirms that the experimental setup only approximately matches the simplified conditions and geometry of the analytical and numerical model.

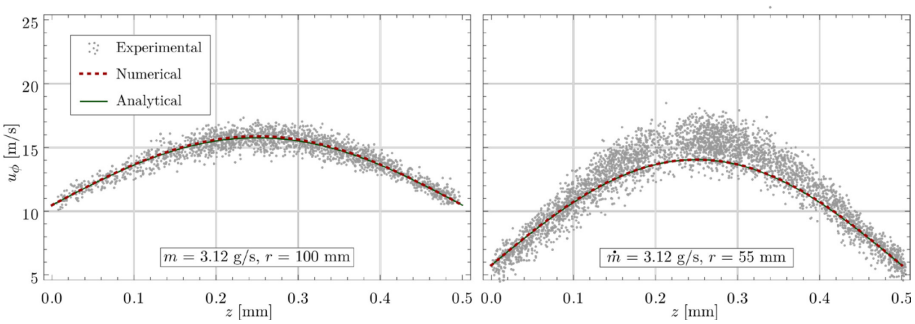

Fig. 3 Tangential velocity profiles at $r = 100mm$ ($R = 0.80$) and $r = 55mm$ ($R = 0.44$).

3 Optimization of key turbine parameters

The analytical solutions for velocity and pressure inside the turbine rotor gap (see chapter 2.1) are cheap to evaluate and therefore effortlessly yield performance maps dependent on the underlying dimensionless parameters. Naturally, the simplifications that govern the analytical model also apply to this investigation, e.g. laminar flow and rotationally symmetric inflow. Dimensionless turbine power and efficiency will serve as indicator values for turbine performance. The power parameter $\dot{W}^*$ for instance generalizes the power output per turbine gap $\dot{W}$:

$$\dot{W}^* = \frac{\dot{W}}{\rho\, u_{r1}^3\, r_1^2} \tag{5}$$

The power parameter arises from the mathematical model by multiplying rotational speed and torque. The latter is equal to twice the disk-surface integral of the shear stress T_ϕ times R^2.

$$\dot{W}^* = 2\Omega \int_0^{2\pi} \int_{R_2}^{R_1} \mathrm{T}_\phi\, R^2\, dR\, d\phi \tag{6}$$

with

$$\mathrm{T}_\phi = \frac{1}{Re} \frac{\partial U}{\partial Z}\bigg|_{Z=\pm 1} \tag{7}$$

The Euler-turbomachinery equation provides the same result whilst avoiding differentiation and integration of the tangential velocity component U.

$$\dot{W}^* = 4\pi\sigma\Omega(U_1 R_1 - U_2 R_2) \tag{8}$$

The isentropic, total to static efficiency serves as measure for turbine efficiency. This way, the kinetic energy of the fluid that leaves the turbine is considered lost, as it is the case for single stage turbines. C_1 represents the absolute velocity at the rotor inlet.

$$\eta_{ts} = \frac{\dot{W}^*}{4\pi\sigma\left(P_2 - \left(P_1 + \frac{C_1^2}{2}\right)\right)} \tag{9}$$

with

$$C = \sqrt{V^2 + U^2 + W^2} \tag{10}$$

The following study aims to provide a brief overview of the turbine parameters, summarized in equation (3). The experimentally examined operating point (see Table 1) serves as starting point. Several surface plots show how each parameter affects the power output and efficiency of the turbine. Each chart depicts the influence of the Reynolds number and one more parameter. All other parameters not mentioned in the charts assume the base values from Table 1. The laminar, transitional and turbulent regions are not yet marked out

in terms of Reynolds Number, thus the charts display the close neighborhood of the starting point conditions, from $Re = 0$ to $Re = 200$.

3.1 Gap width

Fig. 4 shows that the dimensionless power output per rotor gap grows with the dimensionless gap width σ and drops with the Reynolds number. The chart on the right hand side reveals that a small dimensionless gap width is beneficial for efficiency in high Reynolds number flows.

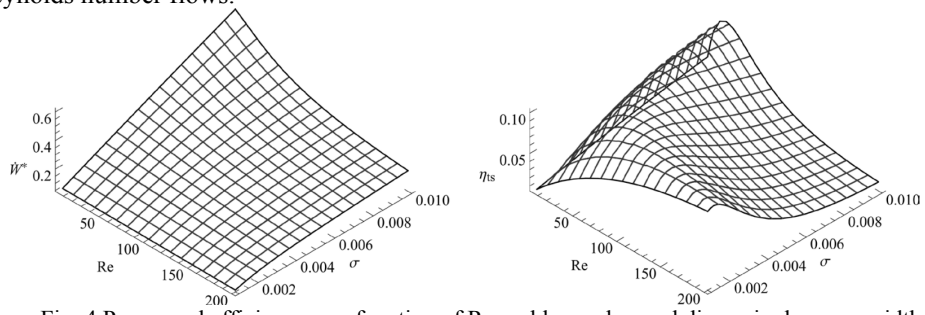

Fig. 4 Power and efficiency as a function of Reynolds number and dimensionless gap width.

3.2 Outlet radius

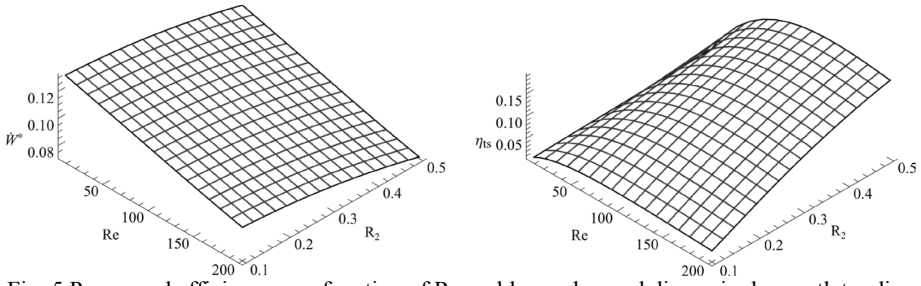

Fig. 5 Power and efficiency as a function of Reynolds number and dimensionless outlet radius.

At high Reynolds numbers, it becomes apparent that a small outlet radius has a positive effect on the power output. The efficency map exhibits opposing trends, i.e. high Reynolds numbers and a big outlet radius result in the best efficiency. In the region of big outlet radii, a weak efficiency maximum arises at about $Re = 100$.

3.3 Inlet angle

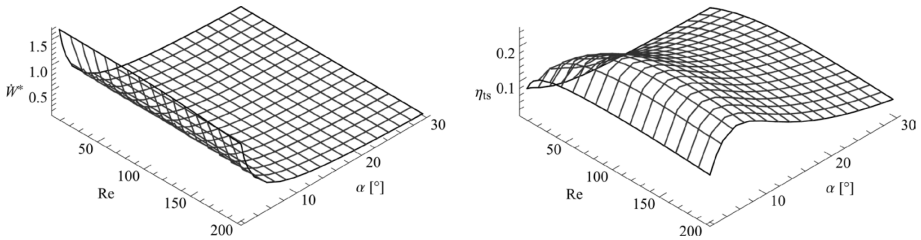

Fig. 6 Power and efficiency as a function of Reynolds number and inlet angle.

A small inlet angle α is good for both the efficiency and the power output of the turbine (see Fig. 6). Only if it drops below 5°, the efficiency drops rapidly.

3.4 Rotational speed

A high dimensionless rotational speed Ω yields a high power output for all Reynolds numbers. High efficiency is generally caused by high Ω and Re. The upper limit of the Ω-axis in Fig. 7 is chosen so that the circumferential speed of the rotating disk surface matches the tangential fluid velocity. This is the case when $\Omega = U_1$.

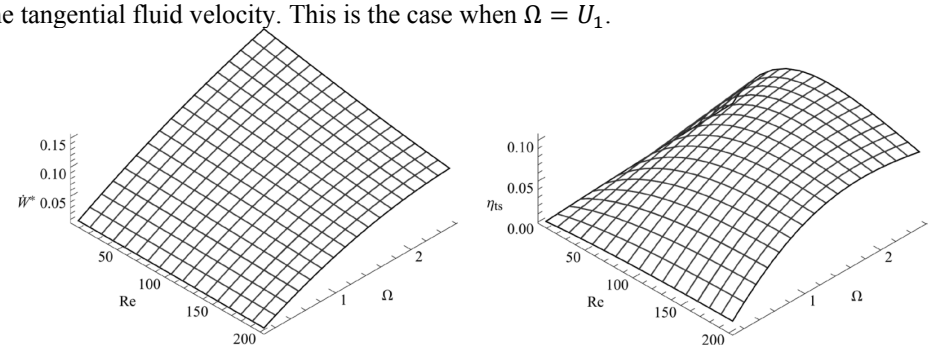

Fig. 7 Power and efficiency as a function of Reynolds number and dimensionless rotational speed.

3.5 Summary

Like any other turbine, a friction turbine is required to work as efficiently as possible while providing as much power output as possible with regard to its size. The analysis of the close neighborhood of the experimentally examined operating point reveals that an efficient turbine exhibits small σ and α, medium Ω and big R_2. Except for α and Ω, the power output follows opposing trends, so that the turbine designer has to find an appropriate compromise.

4 Outlook

The present study provides a very brief overview of the current state of analytical, numerical and experimental research about friction turbines, conducted by the authors. Future efforts will be guided towards a comprehensive design approach for this type of turbomachinery. A new test facility with an application-oriented multigap tesla turbine will test the presented analytical design approach.

References

[1] M. Batista, "Steady flow of incompressible fluid between two co-rotating disks," *Applied Mathematical Modelling,* vol. 35, p. 5225–5233, 2011.

[2] C. Schosser, S. Klingl, S. Lecheler, T. Fuchs, R. Hain, C. Kähler and M. Pfitzner, "Comprehensive investigation of the flow in a narrow gap between co-rotating disks," *European Journal of Mechanics - B/Fluids,* vol. 78, p. 50-61, 2019.

[3] C. Schosser, "Experimental and Numerical Investigations and Optimisation of Tesla-Radial Turbines," *Dissertation, Universität der Bundeswehr, München,* 2016.

[4] C. Schosser, S. Lecheler and M. Pfitzner, "A Test Rig for the Investigation of the Performance and Flow Field of Tesla Friction Turbines," *ASME Turbo Expo 2014: Turbine Technical Conference and Exposition, Düsseldorf, Germany,* no. 45585, 2014.